

Airfoil Flow Experiment on the Duty Cycle of DBD Plasma Actuator

Kengo Asada* , Yoshihiko Ninomiya †

University of Tokyo, Sagamihara, Kanagawa, 229-8510, Japan

Akira Oyama‡ , Kozo Fujii §

Institute of Space and Astronautical Science, JAXA, Sagamihara, Kanagawa, 229-8510, Japan

The parameters of DBD (Dielectric Barrier Discharge) plasma actuator with burst wave (duty cycle) are investigated by the low speed wind tunnel experiment for airfoil. In this paper, influence of burst frequency f^+ , input voltage sine wave frequency f_{base} and burst ratio BR on the stall control are discussed. The experiments are conducted with the conditions $Re_c=44,000, 63,000$. The actuator is applied to NACA0015 airfoil and then flow-fields around the airfoil are visualized by the smoke wire method and pressure around its surface is measured by the multipoint steady pressure measurement. The results show that within the present experimental conditions, the higher f^+ and f_{base} are more effective in the separation control and the smaller BR has the stronger separation control capability in spite of less input energy. In present conditions, the optimum dimensionless burst wave frequency F^+ is 9.1. This result shows the same tendency as the result of Sidorenko, et al.

Nomenclature

BR	Burst ratio, $BR = \frac{T_{on}}{T}$
c	Chord length
C_L	Lift coefficient
D	Drag
f_{base}	Input voltage sine wave frequency
f^+	Burst wave frequency, $f^+ = \frac{f_{base} \times BR}{n}$
F^+	Dimensionless burst wave frequency, $F^+ = \frac{f^+}{U_\infty/c}$
L	Lift
n	Wavenumber for one burst wave cycle
T	Burst wave period
T_{on}	Period of sine wave switch on
U_∞	Free stream speed
V_{ac}	Input voltage sine wave amplitude
x	Coordinate in direction of chord length from the leading edge
α	Angle of attack

*Graduate Student, Department of Aeronautics and Astronautics, 3-1-1 Yoshinodai, student member AIAA.

†Graduate Student, Department of Aeronautics and Astronautics, currently Mitsubishi Heavy Industries, LTD.

‡Assistant Professor, Department of Space Transportation Engineering, 3-1-1 Yoshinodai, AIAA Member.

§Professor, Department of Space Transportation Engineering, 3-1-1 Yoshinodai, AIAA Fellow.

I. Introduction

Planetary exploration airplane has been researched in Japan as well as US as a mean of Mars exploration in the future. Planetary exploration airplane is superior to satellite in respect of the observation data resolution, and to rover in respect of inquiry area. In fact, some design concepts have already been proposed for Mars exploration.^{1,2}

In Martian air, to maintain sufficient lift is a very big problem though gravitational acceleration on Mars is about 1/3 of the earth. It is because the atmospheric density is only 1/100 (i.e. Reynolds number is 1/100) and the speed of sound is about 2/3 of that of earth. Lift coefficient decreases drastically when Reynolds number becomes lower than 10^5 . The Reynolds number of Mars airplanes becomes about only $10^3 \sim 10^5$ because of the low air density and smaller size due to the limitation from the rocket launch ability. Moreover, the capability to deal with various situations like an unexpected state of stall is necessary because there are the strong west wind and the vertical wind in the Mars atmosphere. That is why, high lift device or active flow control device is very important for the Mars airplane. In this paper, DBD plasma actuator is focused as the high lift device, because DBD plasma actuator has a lot of advantages such as simplicity, active control capability, low energy consumption.

DBD plasma actuator is a small flow control device that can be applied to airfoil stall control, reduction of wall surface friction, etc. It is composed of two electrodes and dielectric as shown in Figure 1. Plasma is generated by dielectric barrier discharge in the area between the exposed electrode and the dielectric when alternative current high voltage is applied to both electrodes. Plasma is accelerated by electric field and provide atmosphere with momentum. So the flow which velocity is as small as about several m/sec is induced from the exposed electrode to the insulated electrode.

In recent years, it has been understood that using unsteadiness input voltage that is called “duty cycle” or “burst wave” on DBD plasma actuator achieves a high effect of the separation control saving the input energy.³⁻⁵ Figure 2 shows duty cycle that periodically switches on/off. However, There are no consensus what kind of duty cycle is effective in control of flow separation over an airfoil. The purpose of this paper is to study about the influence of burst frequency f^+ , input voltage sine wave frequency f_{base} and burst ratio BR on the stall control by low speed wind tunnel experiment. The actuator is applied to NACA0015 airfoil. Flow-fields around the airfoil are visualized with smoke and pressure around its surface is measured.

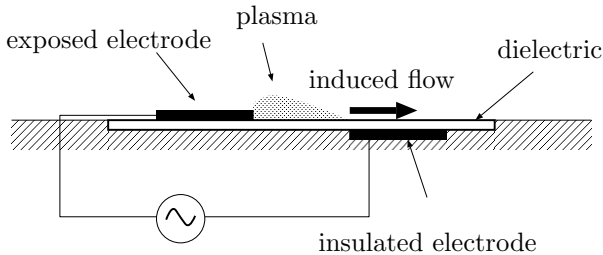


Figure 1. Configuration of the DBD plasma actuator.

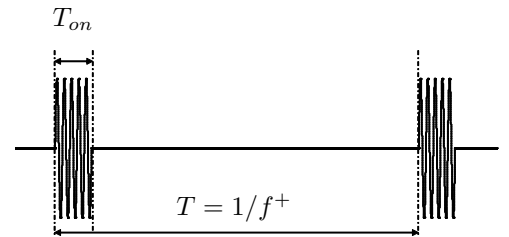


Figure 2. Unsteady duty cycle.

II. Experimental setup

II.A. Experimental apparatus

Low speed inhalation type two-dimensional wind tunnel (R2-DTU: Ready-to-go 2D Testing Unit) at Institute of Space and Astronautical Science, JAXA is used for this research. The test section is 100mm in width, 400mm in height, and 700mm in length. At free-stream speed of 6.6m/sec, turbulence strength in the center is about 0.08%.

Two-dimension wing models made of resin is used for the wind tunnel experiments. The wing has NACA0015 wing section and its chord length and span length are 100mm and 100mm, respectively. Figure 3 and Figure 4 shows the wing models and these are installed DBD plasma actuator vicinity of leading edge. The wing model for the flow-field visualization is coated with mat black paint to avoid reflection of lighting. The wing model for the measurement of pressure has 32 pressure holes on center of span as shown in Figure 5. Two holes of all are located at leading edge and trailing edge, seventeen holes are located at upper surface and thirteen holes are located at lower surface.

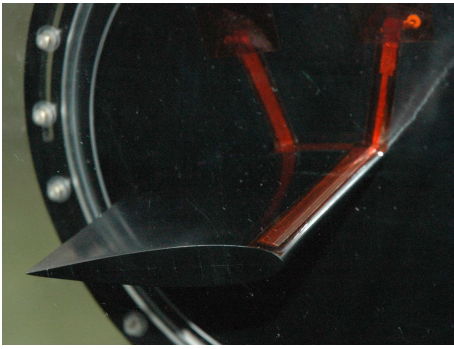


Figure 3. Wing model for visualization with DBD plasma actuator.

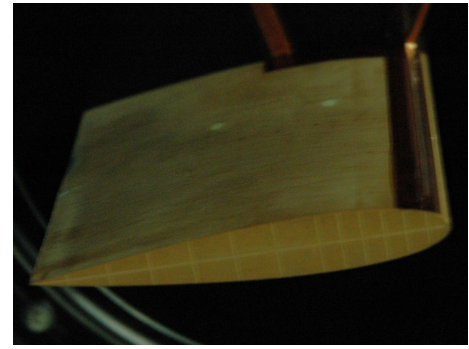


Figure 4. Wing model for pressure measurement with DBD plasma actuator.

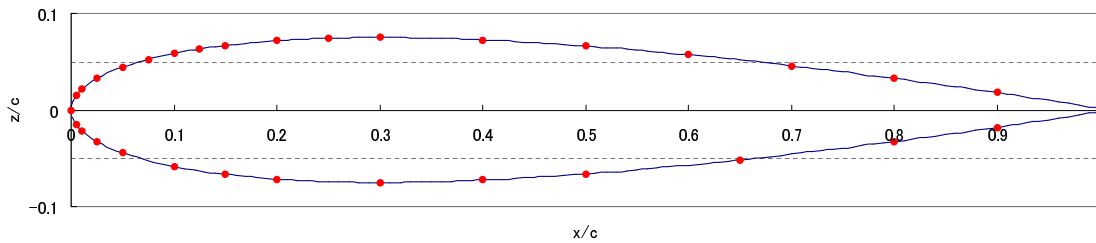


Figure 5. Arrangement of pressure holes on the wing model for the pressure measurement

Polyimide film of $80\mu\text{m}$ (Teraoka Seisakusho,650S, and material thickness $50\mu\text{m}$) for the dielectric and copper tape (3M,Cu-35C) of $70\mu\text{m}$ for the electrode are adopted. They are arranged at the 5% chord length from the leading-edge as shown in Figure 6, because it is reported that to induce higher velocity at the leading edge is the most effective way to control the flow separation in particular condition.⁶ The exposed electrode is connected to high voltage amplifier shown in Figure 7(Trek,model5/80A), while the insulated electrode is connected to Earth, and the originating sine wave from the function generator (NF circuit design and WF1974) is amplified by the high voltage amplifier.

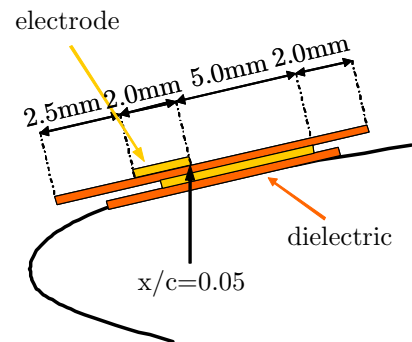


Figure 6. Arrangement of electrode and dielectric.



Figure 7. High voltage amplifier (Trek,model5/80A).

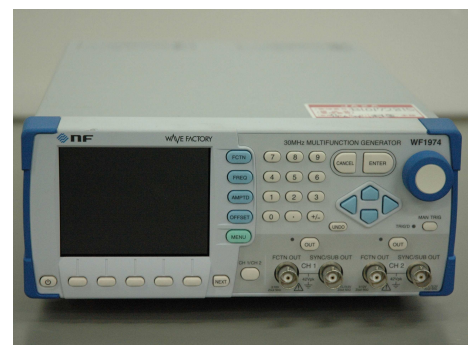


Figure 8. Function generator (NF circuit design and WF1974).

II.B. Experimental cases

Table 1, 2 shows the present input conditions. It should be noted that input energy per unit time increases as f_{base} , V_{ac} or BR increases. Free stream speed is 6.6, 10m/sec in the flow-field visualization cases. Corresponding Reynolds number based on the free stream speed and the chord length is $Re_c = 4.4 \times 10^4, 6.3 \times 10^4$. In the pressure measurement cases, free stream speed is 6.6, 10, 15m/sec. Corresponding Reynolds number based on the free stream speed and the chord length is $Re_c=4.4 \times 10^4, 6.3 \times 10^4, 10.0 \times 10^4$ respectively. In this cases, experiments are carried out mainly at $Re_c=6.3 \times 10^4$ because of the pressure sensor measurement range of confidence.

Table 1. Input voltage conditions in the flow-field visualization experiments

	focused parameter	f_{base} [kHz]	f^+ [Hz]	BR [%]	V_{ac} [kV]
Case1	V_{ac}	6	N/A	100	1.5~4.0
Case2	f_{base}	3,6	N/A	100	2.0~3.0
Case3	BR	6	600	10,50,100	2.0~2.5
Case4	f^+	6	30~600	10	1.5~3.0

Table 2. Input voltage conditions in the pressure measurement experiments

	focused parameter	f_{base} [kHz]	f^+ [Hz]	BR [%]	V_{ac} [kV]
Case1	V_{ac}	6	N/A	100	2.0~3.5
Case2	f_{base}	3,6	N/A	100	2.0~3.5
Case3	BR	6	30~600	10,50,100	2.0~3.0
Case4-1	f^+	6	30~600	10,50	2.0~3.0
Case4-2	f^+	3	30~300	10	2.0~3.0

II.C. Visualization method

Smoke wire method is used for visualizing flow fields. Plasma actuator is driven after starting ventilations. The input condition is changed and a wing surrounding flow when DBD plasma actuator is driven is visualized. The nichrome wire of $\phi 0.1\text{mm}$ is vertically set up at the center of span and 100mm upstream from the leading-edge, the liquid paraffin is spread, and smoke is generated. Pictures of smoke are taken at 1000fps using high-speed camera (TMR,E2).

II.D. Pressure measurement method

Multipoint steady pressure measurement is carried out for measurement of pressure around the wing surface using the multipoint pressure measurement equipment(General Research Institute of Technical Development Co, Ltd. PAB-16PSA). It consists of sixteen semiconductor sensors(Honeywell DUXL05D). Output data is recorded for a second at 1000 Hz sampling frequency and averaged in same condition case. Each condition case is carried out three times. DUXL series's linear and hysteresis error margin is $\pm 0.5\%$ and DUXL05D's measurement maximum range is 5inchAq, so DUXL05D's maximum error ϵ_{max} is shown as below.

$$\epsilon_{max} = 5\text{inchAq} \times 0.01 = 0.05\text{inchAq} = 12.45\text{Pa} \quad (1)$$

This value correspond to $\Delta C_p \approx 0.4$ on $Re_c = 4.4 \times 10^4$ conditions and to $\Delta C_p \approx 0.05$ on $Re_c = 6.3 \times 10^4$ conditions. It is known that the NACA0015 wing flow has a separation bubble on $Re_c = 4.4 \times 10^4$. The pressure measurement resolution ΔC_p need be less than 0.1 to capture the separation bubble, so relatively high Reynolds number is preferable. However, on high Reynolds number flow, the flow-field visualization is difficult. This is why, experiments are carried out mainly at $Re_c=6.3 \times 10^4$ in the pressure measurement cases.

III. Results

III.A. NACA0015 wing characteristic

To understand the stall characteristics of the present NACA0015 wing, the flow-fields around the wing model without the electrode and the dielectric are visualized and pressure around its surface is measured. Figure 9 shows the present NACA0015 wing lift curves on $Re_c = 4.4 \times 10^4, 6.3 \times 10^4, 10.0 \times 10^4$ and a lift curve of the flat plate in potential flow represented as $2\pi\alpha$. These curves C_L values are calculated from the measured pressure values. The present wing flows on each Reynolds number are regarded as stalled at $\alpha=14$ degs, but at $\alpha=12$ degs, the wing flow stalls on $Re_c = 4.4 \times 10^4, 6.3 \times 10^4$ and does not stall on $Re_c = 10.0 \times 10^4$.

Figure 10 shows the time averaged flow-fields during 30msec when angle of attack is 0, 4, 8 and 12degs on $Re_c = 4.4 \times 10^4$. Averaging process was given to the images of consecutive 30frames. At $\alpha=0, 4,$ and 8degs, smoke flows to the trailing-edge in almost parallel to the wing surface. On the other hand, at $\alpha=12$ degs, smoke that passes by the leading-edge flows backward away from the upper surface of the wing, and it can be judged that stall is caused.

Figure 11, 12, 13 show pressure coefficient C_p distribution around the NACA0015. Each figure has similar trend. Peak of negative pressure value at leading edge becomes larger, and the flat C_p distribution from $x/c = 0.4$ to $x/c = 0.4$ which represent a separation bubble at $\alpha = 2$ degs move to leading edge as α becomes higher, At $\alpha = 12$ or 14degs, the flat region of C_p distribution widens, the peak of negative pressure becomes small and trailing edge pressure decrease suddenly. This trend represent the Leading-edge stall and the wing flow stall at $\alpha = 12$ degs on $Re_c = 4.4 \times 10^4, 6.3 \times 10^4$. So following experiments using DBD plasma actuator are carried out at $\alpha=12$ degs to observe that DBD plasma actuator can control stall or not.

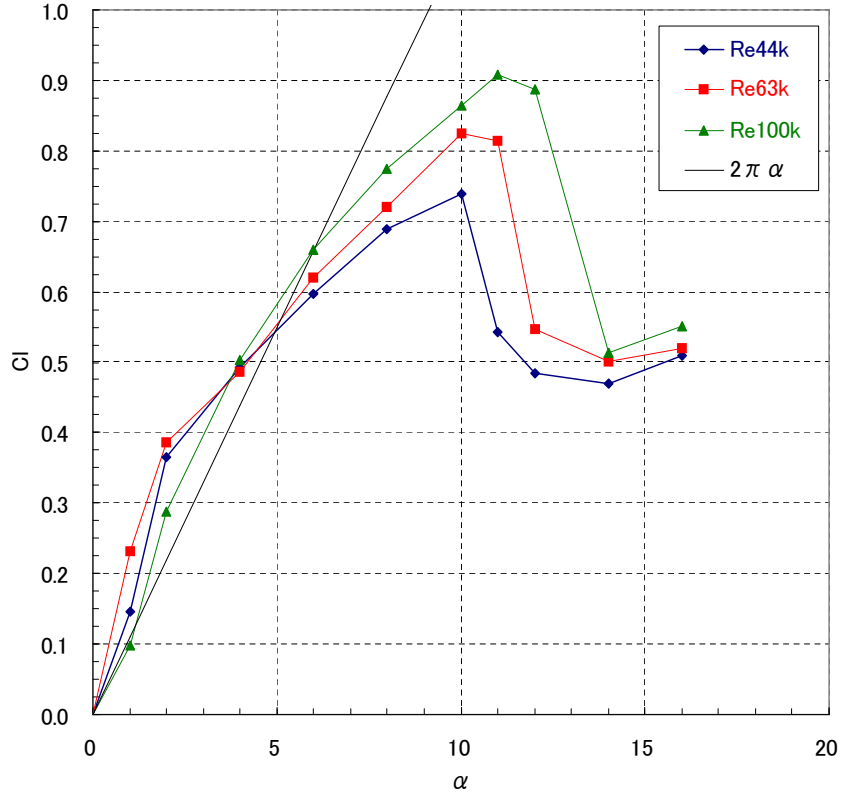
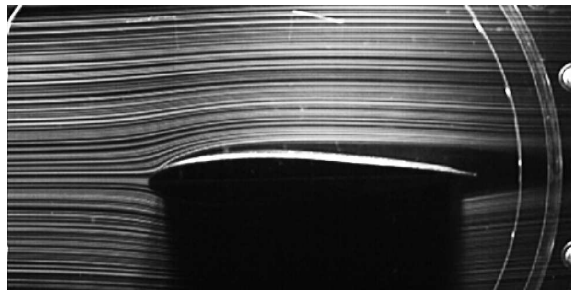
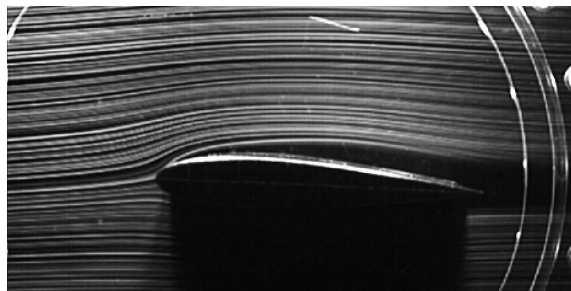


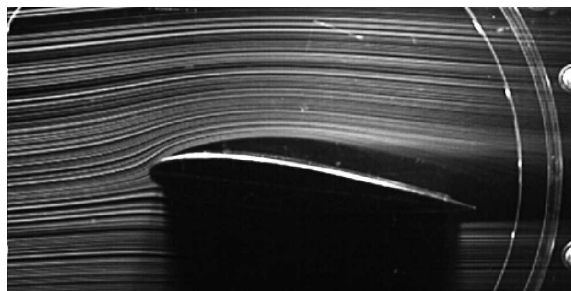
Figure 9. NACA0015 lift curves ($Re_c = 4.4 \times 10^4, 6.3 \times 10^4, 10.0 \times 10^4$).



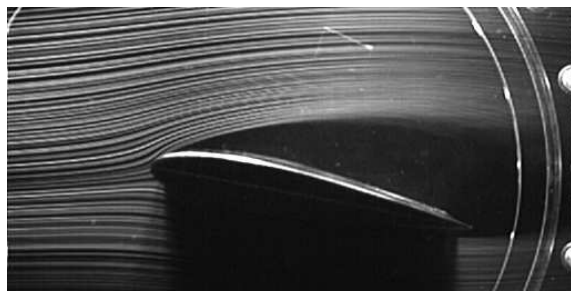
(a) $\alpha=0\text{deg}$



(b) $\alpha=4\text{degs}$

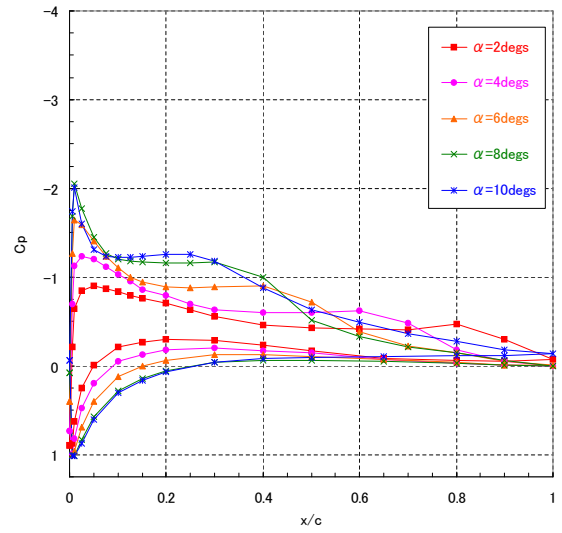


(c) $\alpha=8\text{degs}$

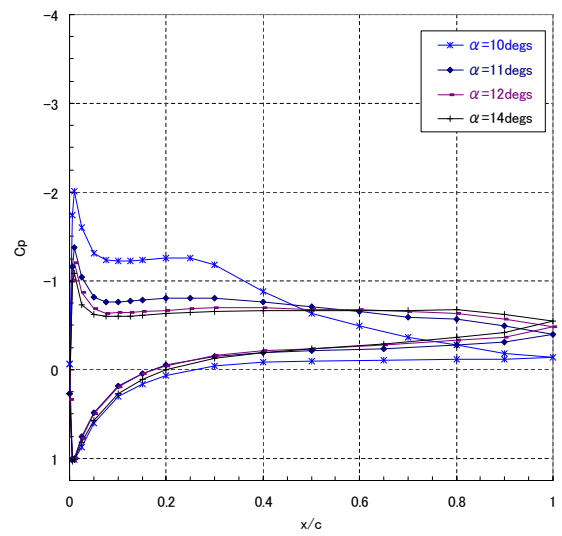


(d) $\alpha=12\text{degs}$

Figure 10. Average flow around the NACA0015 on $Re_c = 4.4 \times 10^4$ ($\alpha=0,4,8,12\text{degs}$ from top to bottom).

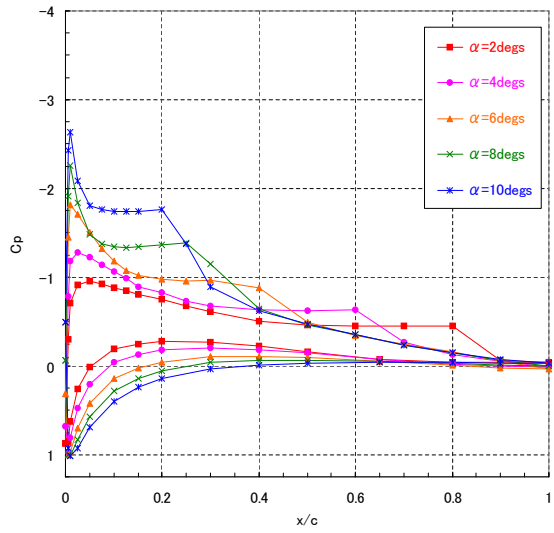


(a) $\alpha = 2, 4, 6, 8, 10\text{degs}$

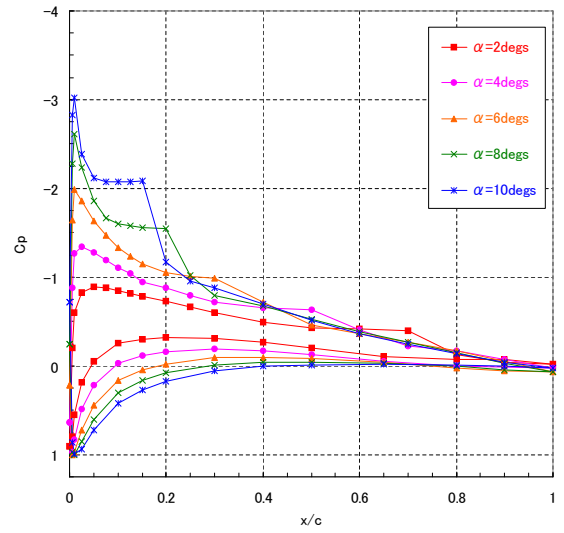


(b) $\alpha = 10, 11, 12, 14\text{degs}$

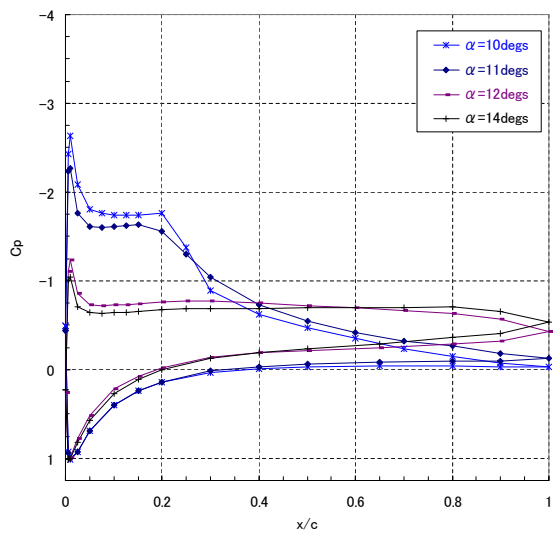
Figure 11. Pressure coefficient distribution around the NACA0015 without DBD plasma actuator on $Re_c = 4.4 \times 10^4$.



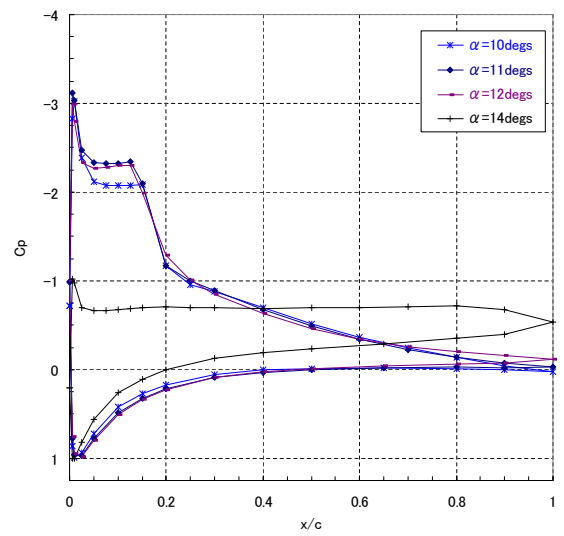
(a) $\alpha = 2, 4, 6, 8, 10$ degs



(a) $\alpha = 2, 4, 6, 8, 10$ degs



(b) $\alpha = 10, 11, 12, 14$ degs



(b) $\alpha = 10, 11, 12, 14$ degs

Figure 12. Pressure coefficient distribution around the NACA0015 without DBD plasma actuator on $Re_c = 6.3 \times 10^4$.

Figure 13. Pressure coefficient distribution around the NACA0015 without DBD plasma actuator on $Re_c = 10.0 \times 10^4$.

III.B. the wing flow with or without DBD plasma actuator

Figure 14 Pressure coefficient distribution around the NACA0015 with and without DBD plasma actuator at $\alpha = 12\text{deg}$ on $Re_c = 6.3 \times 10^4$. “NACA0015” shows the wing without DBD plasma actuator, and “off” shows the wing with it. In the “off” case, the C_p values are connected in the dot-line linearly between $x/c = 0.01$ and $x/c = 0.125$, because the four pressure holes located at $x/c = 0.025 \sim 0.1$ are blocked with dielectric when the DBD plasma actuator is installed on the wing. Pressure coefficient distribution around the wing is a little varied by installing the DBD plasma actuator, but the flow around the wing is regarded as stalled. So installing the DBD plasma actuator is not a problem for following experiments.

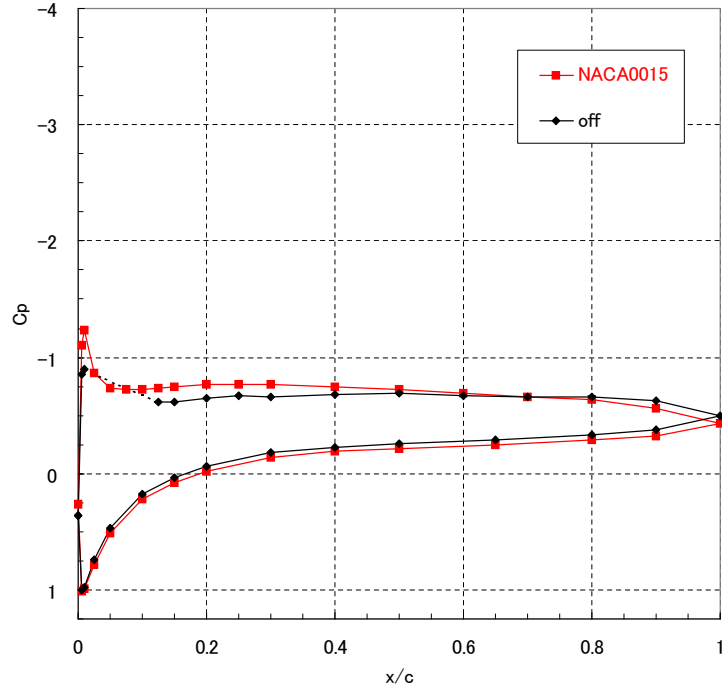
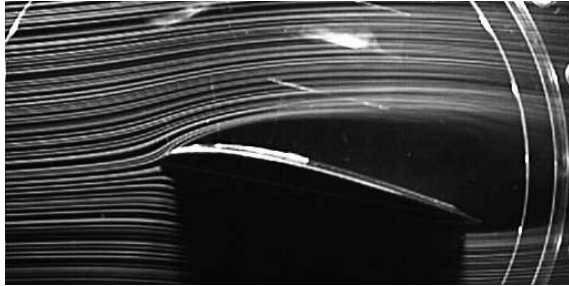


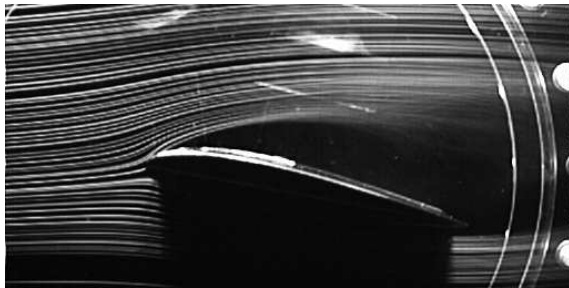
Figure 14. Pressure coefficient distribution around the NACA0015 with or without DBD plasma actuator at $\alpha = 12\text{deg}$ on $Re_c = 6.3 \times 10^4$.

III.C. Stall control in baseline input conditions

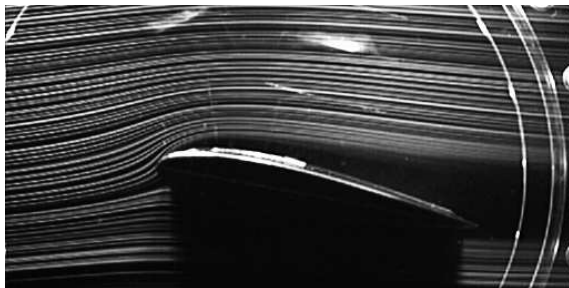
Experiments are carried out according to the input conditions of case1 in Table 1, 2 to understand the effect of the stall control of the DBD plasma actuator without duty cycle. Figure 15 shows the average flow-fields at $\alpha = 12\text{deg}$ on $Re_c = 4.4 \times 10^4$. The top figure shows the average flow when the electrode and the dielectric are installed on the wing, but no input voltage. The one that looks white on the wing at $x/c = 0.1 \sim 0.4$ is wires for the DBD plasma actuator in the wind tunnel wall vicinity. In $V_{ac} = 1.5 \sim 2\text{kV}$, there is not so much effect on the stall control. In $V_{ac} = 2.5\text{kV}$, it was a very unstable flow-field and consistency is not seen in the results of visualizing though a part of effect of the control is seen. In $V_{ac} = 3 \sim 4\text{kV}$, the smoke that passes by the leading-edge flowed in the vicinity of the wing surface is seen by the effect of DBD plasma actuator. The DBD plasma actuator is judged effective in the stall control when the flow-field is changed like this. Figure 16 shows the average flow-fields at $\alpha = 12\text{deg}$ on $Re_c = 6.3 \times 10^4$. On $Re_c = 6.3 \times 10^4$, the DBD plasma actuator is not effective in the stall control in $V_{ac} = 3\text{kV}$, but in $V_{ac} = 3.5\text{kV}$, it is effective in the stall control. it is thought that this is because the free stream dynamic pressure on $Re_c = 6.3 \times 10^4$ is larger than on $Re_c = 4.4 \times 10^4$. Figure 17 shows pressure coefficient distribution around the NACA0015 with the DBD plasma actuator at $\alpha = 12\text{deg}$ on $Re_c = 6.3 \times 10^4$. This result has the same trend as the visualization experiments, although the DBD plasma actuator is effective in stall control on $Re_c = 6.3 \times 10^4$ in $V_{ac} = 3\text{kV}$. These results shows that the higher V_{ac} is more effective in the stall control.



(a) $V_{ac}=0\text{kV}$

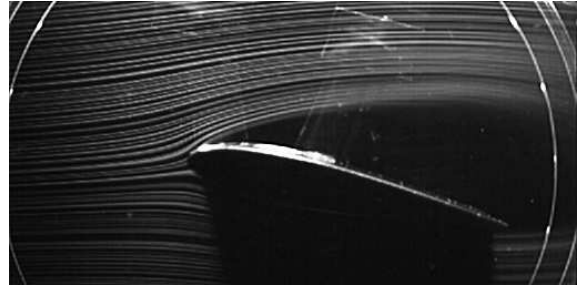


(b) $V_{ac}=2.5\text{kV}$

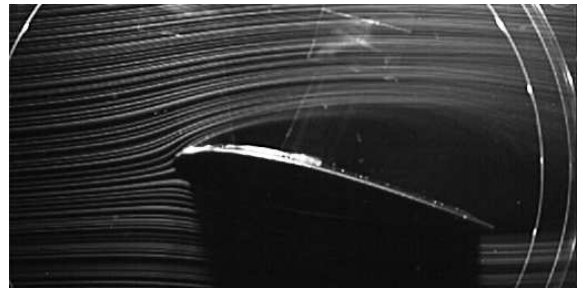


(c) $V_{ac}=3\text{kV}$

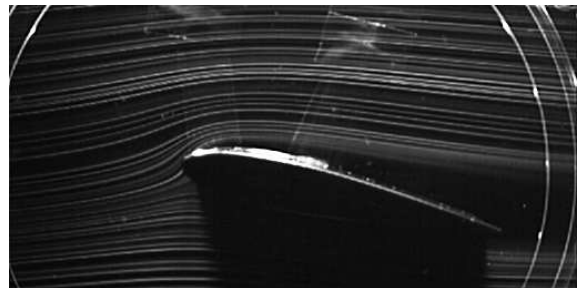
Figure 15. Average flow when stall is controlled
 ($Re_c = 4.4 \times 10^4$, $f_{base}=6\text{kHz}$, $BR=100\%$)



(a) $V_{ac}=0\text{kV}$



(b) $V_{ac}=3\text{kV}$



(c) $V_{ac}=3.5\text{kV}$

Figure 16. Average flow when stall is controlled
 ($Re_c = 6.3 \times 10^4$, $f_{base}=6\text{kHz}$, $BR=100\%$)

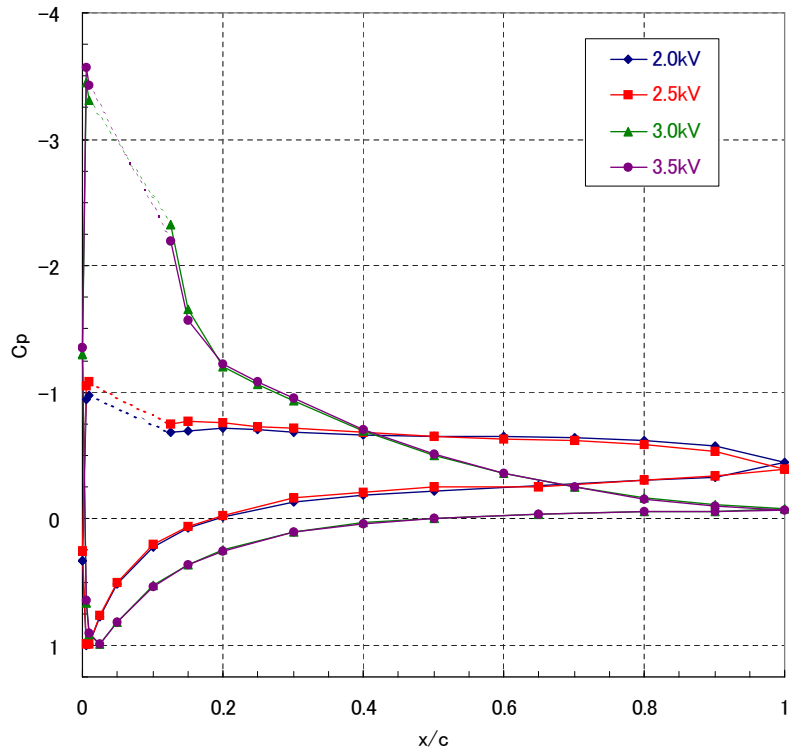


Figure 17. Pressure coefficient distribution around the NACA0015 with the DBD plasma actuator at $\alpha = 12^\circ$ on $Re_c = 6.3 \times 10^4$ ($V_{ac} = 2.0, 2.5, 3.0, 3.5 \text{ kV}$).

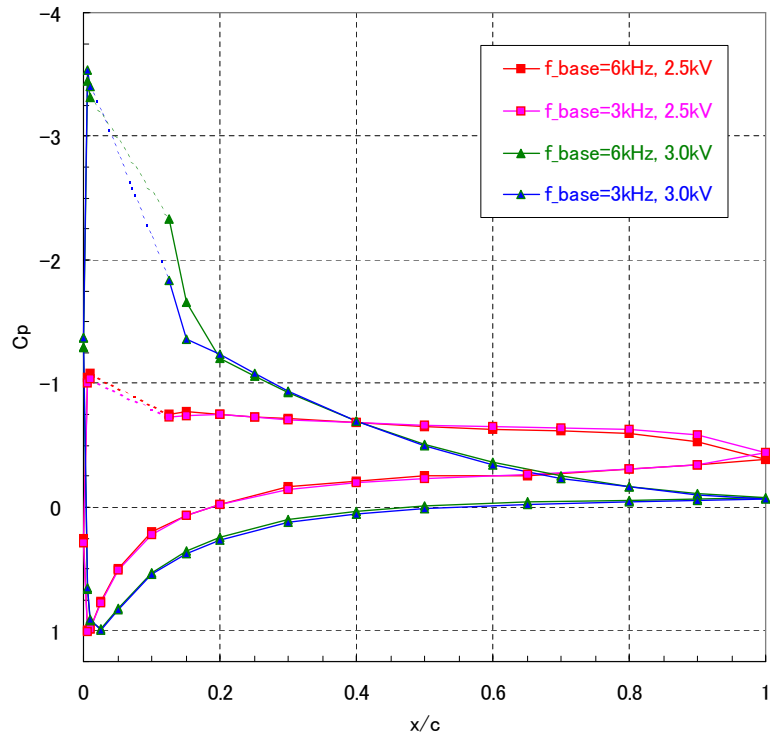


Figure 18. Pressure coefficient distribution around the NACA0015 with the DBD plasma actuator at $\alpha = 12^\circ$ on $Re_c = 6.3 \times 10^4$ ($BR = 100\%$, $f_{base} = 2 \text{ kHz}, 6 \text{ kHz}$, $V_{ac} = 2.0, 3.0 \text{ kV}$).

III.D. Effect of f_{base} on the stall control in baseline input conditions

The stall control experiments are carried out at $f_{base}=3$ and 6kHz to see effect of f_{base} on the stall control. The input condition is Table 1, 2- Case2. A clear difference between $f_{base}=3$ kHz and 6kHz is not seen at the average flow-field in the visualization experiment. Figure 18 shows pressure coefficient distribution around the NACA0015 with the DBD plasma actuator at $\alpha = 12$ degs on $Re_c = 6.3 \times 10^4$ ($BR = 100\%$, $f_{base}=2$ kHz, 6kHz, $V_{ac}=2.0, 3.0$ kV). Seemingly, f_{base} does not affect the stall control, but the $x = 0.125$ region has a little difference in $V_{ac} = 3.0$ kV. In $f_{base}=3$ kHz, negative C_p value is smaller than in $f_{base}=6$ kHz. This is because in $f_{base}=3$ kHz, the leading edge separation bubble is smaller than in $f_{base}=6$ kHz. So it can be judged $f_{base}=3$ kHz is more effective in the separation control than $f_{base}=6$ kHz. It should be noted that input energy increases as f_{base} increases. Therefore f_{base} should be small from the viewpoint of the energy efficiency for the current experimental conditions.

III.E. Effect of BR on stall control

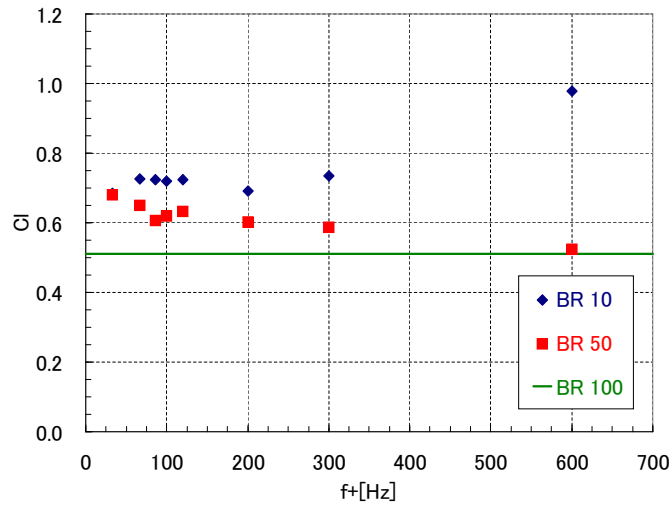
The experiment (Table 1, 2- Case3) with different BR is carried out. The results in the visualization experiment are shown in Table 3 for each BR and each input voltage, where the cases which succeed in separation control are represented by \circ , and the other cases are represented by \times . $BR = 100\%$ means continuous sine wave input. In this experimental conditions, it can be said that the flow separation is the

Table 3. Control result on $Re_c = 4.4 \times 10^4$ by the visualization experiment ($BR = 10, 50, 100\%$, $V_{ac} = 2.0, 2.5$ kV).

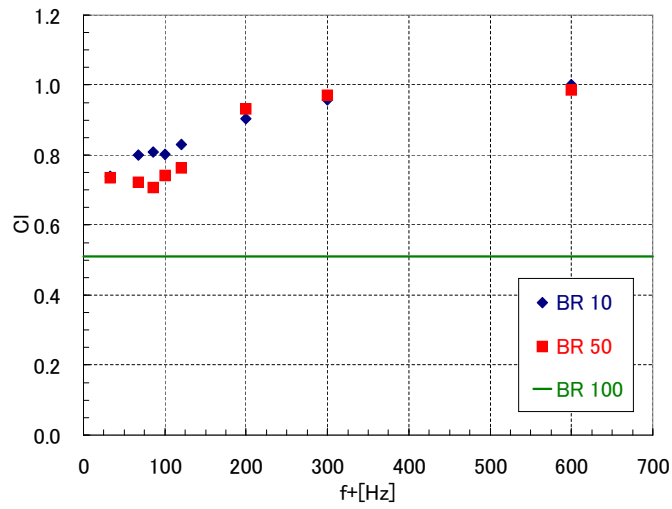
	2.0kV	2.5kV
$BR=100\%$	\times	\times
$BR=50\%$	\times	\circ
$BR=10\%$	\circ	\circ

most controlled at $BR=10\%$. When f_{base} and V_{ac} are constant, the input energy is proportional to BR , so it can be said that the most efficient BR is $BR=10\%$ in present condition.

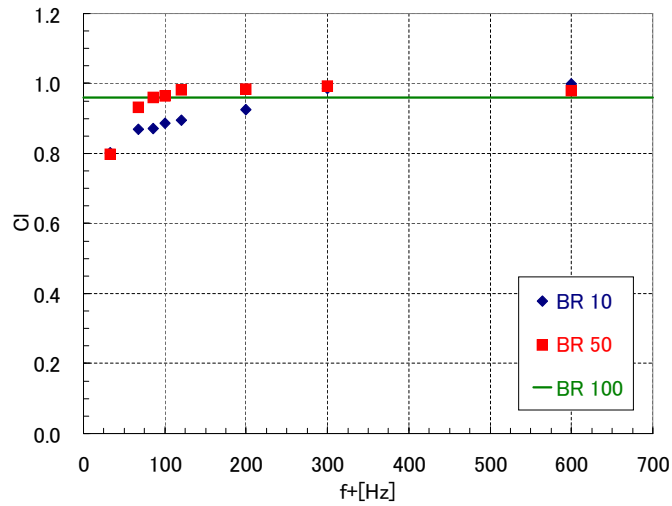
Figure 19 shows C_L vs. f^+ for each V_{ac} in the pressure measured experiment. In the pressure measured experiments, f^+ is varied in addition to the parameters in the visualization experiments. In $V_{ac}=2.0$ kV, $BR = 10\%$ is more effective in the stall control than other BR values. Especially in $f^+=600$, C_L is almost 1.0 in $BR=10\%$, although C_L is about 0.5 in $BR=50, 100\%$. Also in $V_{ac}=2.5$ kV, $BR = 10\%$ is more effective in the stall control than other BR values in $f^+ < 200$ Hz, but in $f^+ \geq 200$ Hz, the stall control effect in $BR = 10\%$ is almost the same effect in $BR = 50\%$. In $V_{ac}=3.0$ kV (This voltage is effective voltage in stall control also in $BR = 100\%$), each BR value has the almost same effect in stall control in $f^+ < 200$ Hz. However in $f^+ \leq 200$ Hz, the burst wave ($BR = 10, 50\%$) effect in stall control is inferior to the sine wave ($BR = 100\%$). These result indicate that there are different stall control mechanisms between the high frequency and low frequency of f^+ .



(a) $V_{ac} = 2.0\text{kV}$



(b) $V_{ac} = 2.5\text{kV}$



(c) $V_{ac} = 3.0\text{kV}$

Figure 19. C_L vs. f^+ on $Re_c = 6.3 \times 10^4$ ($BR = 10, 50, 100\%$, $V_{ac} = 2.0, 2.5, 3.0\text{kV}$, $f^+ = 30 \sim 600\text{Hz}$).

III.F. Effect of f^+ and f_{base} on stall control

Here, influence of the burst frequency f^+ on stall control is discussed. The input conditions are case4 in Table 1, 2. Figure 20 shows minimum voltage required for stall control at each f^+ in the visualization experiments. The required voltage decreases as f^+ increases in the present conditions. This means that larger f^+ is more efficient for the stall control because input energy proportional to V_{ac} if f_{base} and BR are constant.

Figure 21 shows C_L vs. f^+ on $Re_c = 6.3 \times 10^4$ in $BR = 10\%$. Higher f^+ is more effective in stall control, and the C_L value converge with 1.0. In each voltage, $f_{base}=6\text{kHz}$ is more effective in the stall control than $f_{base}=3\text{kHz}$. It is thought that this is because input energy is larger in $f_{base}=6\text{kHz}$ than in $f_{base}=3\text{kHz}$. The maximum f^+ is related to f_{base} . If BR is constant, the maximum f^+ is proportional to the f_{base} . So the higher f_{base} is preferable. Corke, et al. and Göksel, et al. reported that the optimum dimensionless burst wave frequency F^+ is 1. While Sidrenko, et al. reported that the optimum dimensionless burst wave frequency F^+ is $2.6 \sim 14$. In present conditions, the optimum dimensionless burst wave frequency F^+ is 9.1. This result shows the same tendency as the result of Sidorenko, et al.⁴

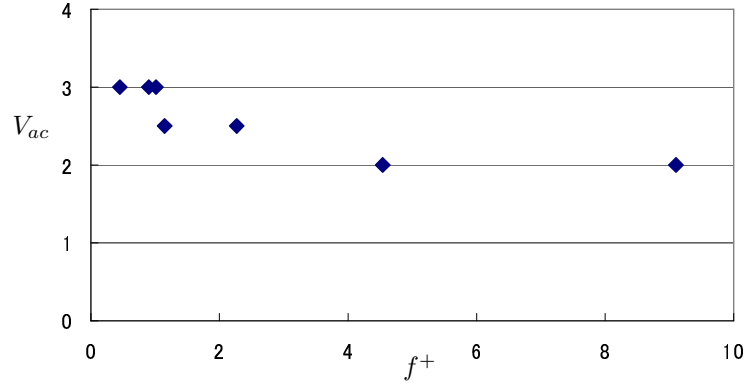


Figure 20. Minimum V_{ac} for stall control vs. f^+ on $Re_c = 4.4 \times 10^4$ ($BR=10\%$, $f_{base} = 6\text{kHz}$).

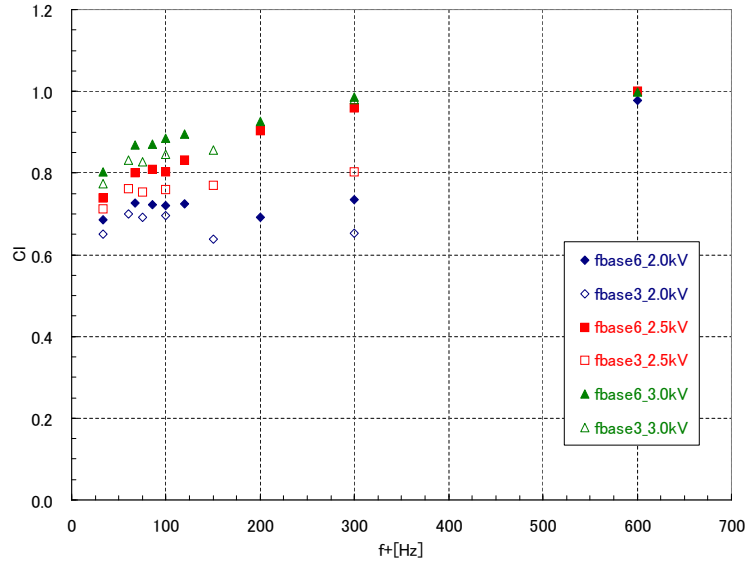


Figure 21. C_L vs. f^+ on $Re_c = 6.3 \times 10^4$ in $BR=10\%$ ($V_{ac}=2.0, 2.5, 3.0\text{kV}$, $f^+ = 30 \sim 600\text{Hz}$).

IV. Conclusions

Within the present experimental condition, the following facts are observed.

1. The higher V_{ac} has more effective in the stall control.
2. The smaller BR has stronger separation control capability in spite of less input energy.
3. The higher f^+ has stronger separation control capability, although f^+ independent of energy consumption.
4. The higher f_{base} has more effective in the stall control, and the maximum f^+ increase with the f_{base} . So the higher f_{base} is preferable.

References

- ¹Guynn, M. D., Croom, M. A., Smith, S. C., Parks, R. W., and Gelhausen, P. A., "Evolution of a Mars Airplane Concept for the ARES Mars Scout Mission," *AIAA Paper 2003-6578*, September 2003.
- ²Tanaka, Y., Okabe, Y., Suzuki, H., Nakamura, K., Kubo, D., Tokuhiko, M., and Rinoie, K., "Conceptual Design of Mars Airplane for Geographical Exploration," *Proceedings of the 36th JSASS Annual Meeting*, Tokyo, April 2005, pp. 61-64, in Japanese.
- ³Göksel, B., Greenblatt, D., Rechenberg, I., Nayeri, C. N., and Paschereit, C. O., "Steady and Unsteady Plasma Wall Jets for Separation and Circulation Control," *AIAA2006-3686*, 2006.
- ⁴Sidorenko, A. A., Zanin, B. Y., Postnikov, B. V., and Budovsky, A. D. e. a., "Pulsed Discharge Actuators for Rectangular Wings Separation Control," *AIAA2007-941*, 2007.
- ⁵Patel, M. P., Ng, T. T., Corke, T. C., Post, M., McLaughlin, T. E., and Suchomel, C. F., "Scaling Effects of an Aerodynamic Plasma Actuator," *AIAA2007-635*, 2007.
- ⁶Tsubakino, D., Tanaka, Y., and Fujii, K., "Effective Layout of Plasma Actuators for a Flow Separation Control on a Wing," *AIAA-2007-474*, 2007.